Published in final edited form as:
Nat Struct Mol Biol. 2016 November ; 23(11): 995–1002. doi:10.1038/nsmb.3296.

E4 Ligase Specific Ubiquitylation Hubs Coordinate DNA Double Strand Break Repair and Apoptosis

Leena Ackermann[#1], **Michael Schell**[#1], **Wojciech Pokrzywa**[1], **Éva Kevei**[1], **Anton Gartner**[4], **Björn Schumacher**[2,3,*], and **Thorsten Hoppe**[1,*]

[1]Institute for Genetics and CECAD Research Center, University of Cologne, Joseph-Stelzmann Str. 26, 50931 Cologne, Germany [2]Institute for Genome Stability in Aging and Disease, Medical Faculty, University of Cologne, Joseph-Stelzmann Str. 26, 50931 Cologne, Germany [3]CECAD Research Center and Center for Molecular Medicine Cologne, University of Cologne, Joseph-Stelzmann Str. 26, 50931 Cologne, Germany [4]Centre for Gene Regulation and Expression, College of Life Sciences, University of Dundee Scotland

[#] These authors contributed equally to this work.

Abstract

The repair of DNA double strand breaks (DSBs) requires tight regulation with the DNA damage response that mediates apoptotic death of damaged cells. Multiple protein ubiquitylation events at the sites of DSBs regulate damage recognition, repair, and signalling processes. However, the spatiotemporal calibration of DNA repair and the apoptotic response remains poorly understood. We identified the E4 ubiquitin ligase UFD-2 in a genetic screen for apoptosis defects after ionizing radiation in *Caenorhabditis elegans*. Following the initiation of homologous recombination (HR) at DSBs, UFD-2 forms foci, which also contain processivity factors including the ubiquitin-selective segregase CDC-48, the deubiquitylation enzyme ATX-3/Ataxin-3, and the proteasome. UFD-2 foci formation requires the recombinase RAD-51 and UFD-2 foci are retained until recombination intermediates are removed by the Holliday junction resolvases GEN-1, MUS-81 or XPF-1. In the absence of UFD-2, the removal of RAD-51-marked DSB repair foci is delayed indicative of inefficient repair. Similarly to *ufd-2* deletion or E4 ubiquitin ligase inactivation, elevated RAD-51 levels lead to defects in DNA damage-induced apoptosis. UFD-2 foci formation also depends on the pro-apoptotic *C. elegans* p53 tumour suppressor homolog CEP-1, suggesting an intricate coordination between DSB processing and the apoptotic response. We establish a central role for the UFD-2 ubiquitin ligase in the coordination between the DNA repair process and the apoptotic response.

[*]Correspondence should be addressed to B.S. or T.H. bjoern.schumacher@uni-koeln.de, Phone: +49 221 478 84202, Fax: +49 221 478 84204; thorsten.hoppe@uni-koeln.de, Phone: +49 221 478 84218, Fax: +49 221 478 84217.

Author Contributions L.A. and M.S. designed, performed and analysed the experiments. W.P. performed *in vitro* ubiquitylation assays. É.K. generated ATX-3 antibody. A.G. and B.S. designed and performed the RNAi screen. B.S. and T.H. supervised the design and data interpretation. L.A., B.S., and T.H. wrote the manuscript. All authors discussed the results and commented on the manuscript.

Author Information Reprints and permissions information is available at www.nature.com/reprints.

The authors declare no competing financial interests.

Europe PMC Funders Author Manuscripts

Introduction

DNA double strand breaks (DSBs) are highly cytotoxic and require the assembly of DNA damage signalling complexes and DSB repair machinery at the DNA breaks 1. In the *C. elegans* germline DSBs are mainly removed through homologous recombination (HR) 2. RAD-51 accumulates at the site of DSBs and mediates the strand invasion into the undamaged template ultimately leading to the formation of cruciform recombination intermediates called Holliday junctions (HJ) 3. HJs can be processed by two major pathways: HJ dissolution via the combined action of Blooms helicase and Topoisomerase TopoIIIα 4, or by resolution of HJ by nucleases acting as resolving enzymes 5. While HJ dissolution predominates in most systems 6,7, in *C. elegans* the GEN-1 resolvase is needed for completion of HR repair of DSBs 8. The resolution of HR intermediates is important for the apoptotic response to DSBs as GEN-1 and HJ processing factors are required for the DNA damage-induced programmed cell death. While the mechanisms for such regulation are not known yet, the C-terminal non-catalytic domain of GEN-1 appears to be important for DNA damage signalling 8,9. The apoptotic response to persistent DSBs facilitates the removal of germ cells in *C. elegans* when DSBs or meiotic recombination intermediates are not repaired, which occurs in the meiotic pachytene zone of the nematode germline (Fig. 1a) 10. DNA damage checkpoint signalling leads to the activation of the *C. elegans* p53 homolog CEP-1 followed by apoptosis induction (Fig. 5a) 11,12. CEP-1/p53 protein becomes available in the late pachytene region of the germline, leading to apoptosis competency of these germ cells. CEP-1 expression in earlier stages of meiosis is translationally repressed by the conserved mRNA binding protein GLD-1 13. Thus, apoptosis is only initiated when aberrant meiotic recombination intermediates or ionizing radiation (IR)-induced DSBs persist in late pachytene cells. It remains, however, unclear how the active repair process coordinates with the apoptotic execution in order to allow sufficient timing for resolving HR intermediates.

Results

Ligase activity of UFD-2 mediates DNA damage induced cell death

To identify new regulators of the apoptotic response to DNA damage, we performed an RNA interference (RNAi) screen targeting 770 genes whose transcription is enriched in the *C. elegans* germline 14 (Fig. 1a). We focused on those genes because in *C. elegans* DNA damage induced apoptosis only occurs in germ cells 10,15. We identified the E4 ubiquitin ligase UFD-2 as to the most prominent candidate resulting from this screen. RNAi against *ufd-2* led to a dose dependent reduction of IR induced apoptosis (Fig. 1b), a phenotype confirmed by analysing *ufd-2(tm1380)* and *ufd-2(hh1)* null alleles (Fig. 1c, d). In contrast, neither developmental apoptosis that occurs during the somatic development of the worm, nor physiological germ cell apoptosis, a background level of germ cell apoptosis that occurs independently of DNA damage, is defective in *ufd-2* mutants (Supplementary Fig. 1a, b).

UFD-2 is a component of the ubiquitin fusion degradation (UFD) pathway first identified in budding yeast 16. Substrate ubiquitylation involves E1 ubiquitin activating, E2 ubiquitin conjugating, and E3 ubiquitin ligase enzymes. UFD-2 defines a class of so-called E4 enzymes, which act by further elongation of pre-existing ubiquitin chains to facilitate

efficient substrate degradation 17–19. Ubiquitin forms chains of varying topology dependent on how molecules are linked to each other, thereby expanding its signalling capacity 20. UFD-2 plays an important role in the process of ubiquitin chain editing and supports proteasomal degradation 19,21. It preferentially makes use of lysine residues 29 and 48 of ubiquitin for autoubiquitylation (Supplementary Fig. 1e). A P951A point mutation in the U-box domain completely blocks the ligase activity of UFD-2 22 (Fig. 1e). To determine if UFD-2 catalytic activity is required for DNA damage-induced apoptosis, we transgenically expressed UFD-2::GFP or UFD-2^{P951A}::GFP in the germline of wild-type or the *ufd-2* deletion background. UFD-2::GFP expression fully restored the apoptotic DNA damage response in *ufd-2(tm1380)* mutant animals (Fig. 1f). In contrast, the catalytically dead mutant UFD-2^{P951A}::GFP showed strongly reduced apoptosis after treatment with 60 Gy IR. The apoptosis defect caused by overexpressing UFD-2^{P951A}::GFP, in a wild-type background indicates that the inactive U-box mutant acts dominant-negatively in response to DNA damage (Fig. 1f).

UFD-2 forms foci after DSB induction

To determine UFD-2 localization, we raised polyclonal antibodies that specifically recognize UFD-2 both by western blot analysis and immunofluorescence staining (Fig. 2a and Supplementary Fig. 2a). Immunostaining revealed that under unperturbed conditions the protein is excluded from nucleoli but otherwise evenly distributed in the *C. elegans* germ line syncytium (Supplementary Fig. 2b). Commencing from late pachytene cells, UFD-2 accumulates at the nuclear periphery resulting into a ring-shaped staining pattern. After IR treatment UFD-2 foci of varying size and number became detectable within the nucleolus (Fig. 2a, b and Supplementary Fig. 2b). The pattern of antibody staining was confirmed by GFP-tagged UFD-2 transgenes (Fig. 2c, d). These UFD-2 foci occur in the mitotic zone as well as in the mid-late pachytene zone of the germline after IR. Given our interest in apoptosis we focussed on UFD-2 foci formation within nucleoli in the pachytene region. Pachytene cells elicit a DNA damage-induced apoptotic response upon DNA damage checkpoint activation, whereas mitotic nuclei in the distal germ line compartment are subjected to cell cycle arrest 10. In contrast to the IR-induced apoptosis defect, the cell cycle arrest, which can be monitored by scoring for enlarged mitotic nuclei due to continuous growth of cellular and nuclear compartments in the absence of cell division (Supplementary Fig. 2b) 10,23, was normally induced in *ufd-2* mutants animals, indicating that the DNA damage checkpoint in general is functional (Supplementary Fig. 1c, d). Unlike IR-induced RAD-51 repair foci which are detectable immediately after damage induction (Fig. 4d) UFD-2 foci accumulated after 12 hrs following damage induction (Supplementary Fig. 2c). We therefore scored UFD-2 foci formation 24 hrs after IR, a time concomitant with full apoptosis activation 10, using both antibodies and GFP transgenes. The number of foci observed in pachytene cells increased from 0-5 foci per germline to more than 15 upon treatment with 60 Gy of IR (Fig. 2a, b and Supplementary Fig. 2b). Collectively, these data suggest that UFD-2 ligase function at first place is dispensable for foci formation (Fig. 2a) but is required to trigger the full apoptotic response.

Ubiquitin-proteasome system factors fine-tune apoptosis response after DNA damage

Since yeast Ufd2 has been implicated in the degradation of the UFD substrates 16,17 and our evidence for UFD-2-mediated ubiquitylation having a role in DNA damage induced apoptosis, we examined if factors associated with the ubiquitin-proteasome system (UPS) accumulate at UFD-2 foci 17,24,25. Hence, we analysed ubiquitin localization 24 hrs after irradiation. In fact, an antibody that recognises conjugated mono- and polyubiquitin chains co-stained UFD-2 foci (Fig. 3a, Supplementary Fig. 3e). Additional staining experiments detected co-localization of the proteasome and the ubiquitin-selective segregase CDC-48/p97 with UFD-2 foci (Fig. 3a). Among other processes, CDC-48/p97 coordinates the degradation of chromatin-associated proteins during DNA replication or DNA repair by extracting ubiquitylated substrate proteins from higher order complexes 26–28. Transgenic over-expression of UFD-2^{C448Y}::GFP, which is not able to interact with CDC-48, but importantly retains ligase activity forms high amount of UFD-2 foci before and after IR treatment (Supplementary Fig. 3f-j). However, UFD-2^{C448Y}::GFP cannot rescue the apoptosis phenotype displayed by *ufd-2* deletion worms (Fig. 3g). CDC-48 guides ubiquitin chain topology by coordinating different UPS-related substrate processing enzymes such as UFD-2 and the deubiquitylation enzyme ATX-3 21. Intriguingly, we also found ATX-3 localized to UFD-2 marked foci (Fig. 3a and Supplementary Fig. 3c, d), suggesting an orchestrated action of UFD-2, ATX-3, and CDC-48 at ubiquitylation hubs in the presence of DNA damage. Interestingly, ubiquitylation activity of UFD-2 is dispensable for the recruitment of ubiquitin processing enzymes. In contrast, apoptosis induction requires ligase activity of UFD-2 as well as its interaction with CDC-48 (Fig. 1e, f and 3b, g).

Given that in yeast and humans, Ufd2/UBE4B mediates elongation of preformed ubiquitin chains, we tested whether UFD-2 collaborates with the E3 ligase HECD-1, the ortholog of budding yeast Ufd4 and human HECTD1 or TRIP12, to trigger DNA damage induced apoptosis 17,29–31. Importantly, loss of HECD-1 prevented UFD-2 foci formation, suggesting ubiquitin-dependent recruitment of UFD-2 (Fig. 3c, d). Supporting the role of UFD-2 focal accumulation in response to DNA damage, apoptosis was reduced in *hecd-1* mutants (Fig. 3e). The apoptosis defect was even more pronounced in *ufd-2; hecd-1* double mutants, indicating that the activity of both enzymes is required to achieve a full apoptotic response (Fig. 3e). In contrast, the deubiquitylation enzyme ATX-3 counteracts UFD-2 recruitment as both UFD-2 foci formation and apoptosis (Fig. 3d, f) was increased in *atx-3* mutants (Fig. 3f). Accordingly, the excessive DNA damage-induced apoptosis occurring in *atx-3* mutants was suppressed in *ufd-2; atx-3* double mutant worms (Fig. 3f). In support of this notion, the number of ubiquitin foci per germline is decreased in *hecd-1*, whereas it is increased in *atx-3* (Supplementary Fig. 3k). We therefore conclude that the apoptotic response to DNA damage is regulated by ubiquitylation signals defined by UFD-2 that cooperates in this response with HECD-1 and ATX-3.

UFD-2 supports RAD-51 dissociation from repair sites after DNA damage

We next analysed if UFD-2 affects the DNA repair process in addition to apoptosis. In contrast to DSB induction by IR, UV irradiation did not result in formation of UFD-2 foci consistent with a specific role of UFD-2 in DSB repair (Supplementary Fig. 3a). In line with this observation we found that RPA-1::GFP and BRD-1::GFP HR proteins 32,33 accumulate

in UFD-2 foci 24 hrs after IR treatment (Fig. 4b). Furthermore, IR of L4 staged *ufd-2* mutant larvae resulted in reduced embryonic survival in the ensuing generation (Supplementary Fig. 3b). To establish whether *ufd-2* promotes the processing of DNA repair intermediates we analysed the kinetics of RAD-51 foci. While both wild-type and *ufd-2* mutants accumulated an equal amount of RAD-51 positive nuclei one hour after IR, twice as many RAD-51 stained nuclei persisted 16 hrs later in *ufd-2* mutants (Fig. 4d). The delay in RAD-51 foci dissociation that temporally coincides with UFD-2 foci formation indicates that UFD-2 might contribute to resolution of repair intermediates.

UFD-2 coordinates DSB repair with apoptotic response

We further investigated the role of DSB repair in UFD-2 foci formation. Impairment of HR in *rad-51* deletion worms blocked UFD-2 foci formation. Conversely, *rad-54* deletion that inhibits removal of RAD-51 from DNA during HR repair 34, causes an accumulation of UFD-2 foci (Fig. 5b). Furthermore, deletion of the *gen-1*, *mus-81*and/or *xpf-1* HJ resolvases led to the accumulation of high levels of UFD-2 foci (Fig. 5c and Supplementary Fig. 4a). These results indicate that HR needs to commence for UFD-2 foci to form and UFD-2 foci are only dissolved once HR is completed (Fig. 5b).

As *ufd-2* mutant worms displayed reduced apoptosis, we assessed whether apoptotic signalling was affected in *ufd-2* mutant worms. The apoptotic core machinery is conserved from *C. elegans* to the mammalian system. The p53 homologue CEP-1 induces transcription of the two BH3-only proteins EGL-1 and CED-13 13,35, which bind to the only Bcl2-like protein CED-9. As a consequence, the inhibitory effect of CED-9 on the Apaf1-like CED-4 is overruled and CED-4 activates the caspase CED-3, which executes the cell death (Fig. 5a) 36. In view of the ubiquitin ligase activity, we tested whether CEP-1 protein accumulates after damage induction in the absence of UFD-2. However, in wild-type and *ufd-2* mutant worms CEP-1 protein was equally upregulated 2-fold upon 60 Gy irradiation (Supplementary Fig. 4b, c, d). Additional evaluation of mRNA transcripts of the CEP-1 target gene *egl-1* showed a comparable transcriptional upregulation in both genotypes 4 and 24 hrs after damage infliction (Supplementary Fig. 4d). After having established that CEP-1 activation occurs independently of *ufd-2*, we wondered if UFD-2 foci formation might be dependent on CEP-1. Strikingly, loss of CEP-1 prevented UFD-2 foci induction after IR (Fig. 5d), whereas UFD-2 protein expression remained unaffected (Supplementary Fig. 5b). Consistently, a double mutant of the two pro-apoptotic CEP-1 effectors, *egl-1; ced-13* phenocopied the *cep-1* defect in UFD-2 foci formation after DNA damage (Fig. 5d and Supplementary Fig. 5a). To further correlate CEP-1 activity and UFD-2 foci formation, we enhanced CEP-1 activity by employing a *gld-1* mutation, previously shown to lead to elevated CEP-1 levels and activity 13. *gld-1* mutants indeed displayed strongly elevated number of UFD-2 foci, supporting the role of CEP-1 in promoting UFD-2 focal accumulation. The *cep-1; gld-1* double mutant displayed a similar number of UFD-2 foci as wild-type germ cells (Fig. 5c and Supplementary Fig. 5a). One potential explanation for the failure of *cep-1* to completely suppress the foci formation in *gld-1* might be the numerous additional target mRNAs of GLD-1 37,38. Of note, the failure of *cep-1* to initiate apoptosis is not correlated to its repair capacity. DNA repair assessed by embryonic survival is not perturbed in *cep-1*, but rather slightly increased in *gld-1* mutants (Supplementary Fig. 5c). In

ced-3 and *ced-4* mutant worms UFD-2 foci generated normally (Fig. 5d), emphasising the necessity of CEP-1 rather than apoptotic signalling in general for UFD-2 foci formation. Taken together, UFD-2 foci formation depends on pro-apoptotic CEP-1 signalling but does not affect CEP-1 protein levels. Thus, UFD-2 seems to act downstream of pro-apoptotic signalling mediated by CEP-1 and EGL-1/CED-13.

We further tested a possible correlation between the effect of UFD-2 on DNA damage and apoptosis. Germline-specific expression of UFD-2::GFP in transgenic *ufd-2* deletion mutants rescued the delay of RAD-51 removal from DNA. In contrast, increased RAD-51 retention occurred in moderately RAD-51::GFP overexpressing worms after 24 hrs of IR compared to wild-type (Fig. 6a). Nevertheless, this line possesses normal repair capacity as assessed by embryonic survival after IR (Supplementary Fig. 6c). Of note, loss of *atx-3*, important for restriction of UFD-2 foci and apoptosis execution after DNA damage, showed decreased RAD-51 retention 16 hrs after IR (Supplementary Fig. 4e). Obviously, the amount of retained RAD-51 foci negatively correlated with the apoptosis response (Fig. 6a, b). As control, *ufd-2* mutants were crossed with *rad-51*. Similarly, RNAi depletion of RAD-51 in *ufd-2* mutants or RAD-51::GFP expressing worms or treatment with the RAD-51 inhibitor B02 39reverted the apoptosis phenotype of *ufd-2* deletion mutants or the RAD-51 overexpression line (Fig. 6c, d, Supplementary Fig. 6a, b), suggesting that RAD-51 accumulation directly blocks apoptosis signalling. In summary, these observations suggest that UFD-2 contributes to resolution of DNA repair sites, possibly by supporting the repair process directly or regulating the dynamics of repair proteins in specified degradation centres. Our data indicate that loss of E4 activity might cause the retention of RAD-51 on the DNA, which manifests in a transient block of apoptosis (Fig. 7).

Discussion

In this study we uncovered a ubiquitin dependent process that facilitates the communication between DNA repair and the apoptotic response. We identified the E4 ubiquitin ligase UFD-2 as a central regulator for the spatiotemporal coordination of both processes. Our data suggest that defects in timely proceeding of HR either by failure to resolve HJs as previously demonstrated 8,9 or by aberrant retention of RAD-51 at the chromatin caused by loss of UFD-2 as shown here, halt the apoptotic response. Conversely, RAD-51 filament assembly and pro-apoptotic signalling by the tumour suppressor CEP-1/p53 are both required for the formation of UFD-2-specific hubs that are defined by proteolytic factors of the UPS machinery. We propose that these degradation hubs calibrate the DNA repair status with apoptotic activity via modulation of ubiquitin signalling. Since the E3 ligase HECD-1 is required for UFD-2 hub formation and apoptosis execution, we further propose that E4 activity 17,30,40 is providing an additional layer of regulation by editing ubiquitin chain topology. The human E4 homolog UBE4B cooperates similarly with the HECT domain E3 ligase TRIP12 in substrate ubiquitylation, suggesting the existence of a conserved signalling pathway 29. In support of this idea, TRIP12 fine-tunes ubiquitin controlled events at DSBs 41 and recent reports linked UBE4B to different cancer types, highlighting the relevance of ubiquitin signalling in the decision between DNA damage and apoptosis response 42–45. Not only during meiotic recombination and DSB repair in germ cells but also during the maintenance of tissue integrity following DNA injury the apoptotic response requires timely

adjustment to on-going activity of DNA repair processes particularly when they are as complex as HR. Defects in the both DNA repair and apoptosis are especially relevant in tumour formation. Thus, understanding the conserved role of UFD-2/UBE4B in response to IR induced DNA damage might open new therapeutic directions for drug development and cancer treatment.

Methods

C. elegans strains

C. elegans strains were cultured at 20 °C on nematode growth medium (NGM) and fed with *Escherichia coli* (*E. coli*) strain OP50 according to standard procedures 46. The Bristol strain N2 was used as wild-type. Mutants and transgenic animals used in this study are listed in the following: *mus-81(tm1937) I, rad-54&snx-3(ok615) I/hT2 [bli-4(e937) let-?(q782) qIs48] (I;III), cep-1(lg12501)I, ced-1(e1735)I, gld-1(op236)I, ufd-2(tm1380)II, ufd-2(hh1)II, xpf-1(tm2842) II, gen-1(tm2940)III, ced-4(n1162) III, hecd-1(tm2371)IV, rad-51(ok2218) IV/nT1[qIs51](IV;V), ced-3(n717) IV, atx-3(gk193)V, egl-1(n1084n3082)V; ced-13(tm536)X, , Is[rad-51::GFP:3xFLAG], gla-3(op216)I, hus-1(op241)I, unc-119(ed3)III; gtIs[unc-119(+), Ppie-1::GFP::rpa-1::pie-1-3'UTR], hhIs121[unc-119(+), Pmex-5::ufd-2::GFP::tbb-2 3'UTR], hhIs135[unc-119(+), Pmex-5 (w/o ATG)::ufd-2 (w/o TAA, P951A)::(Gly)5Ala::gfp F64LS65T(w introns/stop)::tbb-2 3'UTR], hhIs134[unc-119(+), Pmex-5::ufd-2 (C448Y)::GFP::tbb-2 3'UTR].*

The transgenic lines *hhIs121, hhIs134* and *hhIs135* were generated for this study. Briefly, fosmid WRM0621dE05 was used as template to obtain the genomic sequence of *ufd-2* that was cloned together with ppJA252, pJA257 into pCG150 containing the unc-119(+) marker for selection of transgenic worms 47. *ufd-2* was modified by directed mutagenesis to create *ufd-2*^{P951A} or *ufd-2*^{C448Y}. The constructs were bombarded into *unc-119(ed4)III* mutants as described previously 48.

Ionizing radiation

Synchronized hermaphrodites were grown until L4 stage and irradiated with the corresponding dose (Radiation source: 120-kV X-rays (25 mA; 0.5mm Alu-filter; ISOVOLT 160 M1/10-55, GE Sensing & Inspection Technologies) or Biobeam 8000 using Cs137 as radiation source).

RNAi treatment

RNA interference was performed using the feeding method 49. Three P0 worms were placed on IPTG (isopropylthiogalactoside) and ampicillin-containing NGM-plates seeded with *E. coli* [HT115(DE3)] expressing double-stranded RNA (dsRNA) and incubated at 15°C for 72 hrs. Three single F1 worms were transferred each to a new, freshly seeded plate and allowed to lay eggs for approximately 20 hrs. F1 worms were removed and F2 worms were allowed to grow up to the L4 stage, treated with ionizing radiation and analyzed for radiation induced apoptosis. Clones in RNAi feeding vectors were provided by Marc Vidal of Dana Farber Cancer Center.

Apoptotic corpses

For physiological apoptosis analysis, synchronized L1 larvae were grown until L4 stage. Apoptotic corpses were scored 24 hrs later. For this, worms were mounted on 3% agar pads, paralyzed with 60 nM NaN_3 and analysed via DIC microscopy 50. For DNA damage induced apoptosis worms were subjected to IR at L4 stage before apoptosis was evaluated 24 hrs later. Developmental apoptosis was assessed in L1 larvae. Therefore worms were grown until day one adulthood. 100 worms were transferred to a NGM-agar plate without *E. coli* and allowed to lay eggs until they were removed again after 1 h. Freshly hatched L1 larvae were scored for apoptotic corpses 51.

UFD-2 foci

Synchronized worms were grown until L4 larvae stage and irradiated with 0 and 60 Gy. 24 hrs later, germlines were isolated and immunostained. Number of UFD-2 foci was scored in all focal planes in pachytene germ cells. One germline per worm was scored.

Protein expression and purification

cDNAs encoding *ufd-2b, ufd-2b*^{C448Y} and *ufd-2b*^{P951A} were cloned into the pET-21d expression vector (Novagen) and pGex4T1 (GE Healthcare). Recombinant proteins were expressed in *Escherichia coli* strain BL21 Codon Plus (Novagen) and purified using the ÄKTA purifier system (GE Healthcare).

Antibody production

His-tagged purified proteins (UFD-2, ATX-3[21]) were used for immunization of rabbits and anti-sera were affinity purified using respective GST-tagged recombinant proteins (BioGenes).

Preparation of worm lysates

Synchronized L1 larvae were grown on NGM-agar plates with OP50 bacteria until they reached adulthood. Worm lysates used for SDS-PAGE were either prepared from a distinct number of worms (n=150) or by washing worms from NGM-agar plates followed by multiple washing step with M9 buffer (3 g/l KH2P04, 6 g/l Na2 HPO4, 5 g/l NaCl, 1 mM Mg S04 (added after sterilization)), until bacteria were removed. The samples were heated to 95°C for 5 min and subsequently shock-frozen in liquid nitrogen. After thawing, samples were subjected to sonication (two times for 15 s, on ice; 50% power; Sonopuls UW 2200, Bandelin) and taken up in 4 x SDS sample buffer followed by centrifugation at 15,000 rpm for 10 min.

Immunotechniques

Immunostaining of isolated germlines was done according to the ‘freeze-crack’ protocol. Worms were dissected onto polylysine-coated slides (Thermo Scientific) in 60 nM NaN_3 to isolate germlines and fixed in fixation buffer (3.7 % Formaldehyde, 0.2 % Tween 20) for 10 min with subsequent shock freezing in liquid nitrogen. This was followed by incubation in 1:1 mixture of methanol and acetone at -20 °C for 10 min. Germlines were permeabilized 3 times in 1 % PBS-Triton X-100 for 20 min followed by washing in 0.1 % PBS-Tween 20

(PBS-T) for 10 min and blocking in 10 % goat serum in 0.1 % PBS-T. A specific staining protocol was followed for GFP-expressing lines avoiding freezing. Isolated germlines were fixed with fixation buffer for 10 min in PCR tubes, directly followed by permeabilization and blocking as described above. Germlines were incubated with primary antibody overnight at 4 °C (anti-UFD-2 1:3,000, anti-CDC-48 1:12,000, anti-RAD-51 1:350 (Novus), anti-FK2-ubiquitin 1:100 (Millipore), anti-Proteasome 20S alpha 1+2+3+5+6+7 antibody 1:300 (abcam), anti-ATX-3 1:700). Incubation with the fluorescently labelled secondary antibodies (Life Technologies; 1:200) or GFP-booster (ChromoTek; 1:400) was done at room temperature for 1 h. Germlines were mounted in DAPI Fluoromount-G medium (SouthernBiotech). For western blotting, worm lysates were separated by SDS–polyacrylamide gel electrophoresis (SDS–PAGE) and transferred to nitrocellulose membranes (Whatman, Protran). Membranes were blocked in 1x Roti-Block (Roth) and incubated with the primary antibodies overnight at 4 °C in Roti-Block (Roth; anti-UFD-2 1:20,000, anti-ATX-3 1:10,000, anti-CEP 1:15,000, anti-tubulin 1:5000 (Sigma-Aldrich, clone DM1A). Incubation with fluorescently labelled secondary antibodies (1:10,000) was done at room temperature, before detection of signals using the Li-Cor Odyssey scanner. Quantification of signal intensities was done using the Odyssey V4.0 software (Li-Cor). The uncropped versions of western blots that have been used to assemble the main figures are collected in Supplementary Fig. 6.

Microscopy and image acquisition

Immunostained germlines were imaged with AxioImager.M1/Z1 microscope with Apoptome equipped with an AxioCam MRm camera (Carl Zeiss). To allow direct comparison of signal intensities, images were recorded under identical conditions. Processing of selected pictures was done in ZEN2011 and ImageJ.

In vitro ubiquitylation assay

UFD-2b::His, UFD-2b^{C448Y}::GST and UFD-2b^{P951A}::His fusion proteins were expressed in BL21-AI *E. coli* strain and lysed in buffer A (50 mM Tris pH 7.5, 250 mM NaCl, 5 mM DTT, 1% Triton X-100, 2 mM PMSF and protease inhibitor mix; Roche). 10 μg of the aforementioned bacterial lysate was mixed with E1 (25 ng), E2 (Let-70; 400 ng), 2 μg of FLAG::ubiquitin, energy regenerating solution (Boston Biochemicals) and ubiquitin conjugation reaction Buffer (Enzo Life Sciences). Samples were incubated at 30 °C for 1.5 h, terminated by boiling for 5 min with SDS-sample buffer, and resolved by SDS-PAGE followed by immunoblotting using anti-UFD-2 antibodies to monitor ubiquitylation of UFD-2.

Persistence of RAD-51 foci after IR

Synchronized worms were grown until L4 larvae stage and irradiated with 0 and 20 Gy. 1 to 48 hrs later, germlines were isolated and immunostained. Z-stacks were taken of late pachytene cells of the germline. Two focal planes covering the upper and lower part of the germline were subjected to analysis by scoring each plane for RAD-51 positive cells in the last 25 nuclei.

RNA isolation and real-time PCR

Total RNA was isolated using TRIzol (Invitrogen) and Qiagen RNeasy kit. Briefly, worms were washed off the plates using M9 buffer (3 g/l KH_2P0_4, 6 g/l Na_2 HPO_4, 5 g/l NaCl, 1 mM Mg $S0_4$ (added after sterilization)) and 600 μl TRIzol, and silica beads (1 mm diameter) were added to the samples and homogenized by Precellys tissue homogeniser. Chloroform was added and samples were vortexed vigorously before phase separation through centrifugation. The aqueous phase was transferred on the Qiagen RNeasy Mini spin column and RNA was isolated according to manufacturer's instructions. cDNA was synthesized using 200 ng total RNA and the High-Capacity cDNA Reverse Transcription Kit (Applied Biosystems). Gene expression levels were determined by real time PCR using Brilliant III Ultra-Fast SYBR Green QPCR Master Mix (Agilent Technologies) and Biorad CFX96 Real-Time PCR Detection System. Relative gene expressions were normalized to *tbg-1* (F58A4.8) mRNA levels. In the experiment three biological and three technical replicate samples were analyzed. The primer sequences used in the RT–PCR reactions are the following: *tbg-1* forward: 5′-GTACACTCCACTGATCTCTGCTGACAAG-3′, *tbg-1* reverse: 5′-CTCTGTACAAGAGGCAAACAGCCATG-3′ 52, *egl-1* forward: 5′-TACTCCTCGTCTCAGGACTT-3′, *egl-1* reverse: 5′- CATCGAAGTCATCGCACAT-3′.

Radiation sensitivity

To determine the radiation sensitivity, L4-stage hermaphrodites were irradiated with a single dose of IR as indicated. After 12 hrs, worms were transferred to fresh plates (three worms per plate, five plates in total) and allowed to lay eggs for 5 hrs. After this period, adults were removed and 24 hrs later the number of hatched and unhatched embryos was scored. As a control for DNA damage sensitivity, a heterozygous deletion mutant lacking *rad-51* on one chromosome was used.

Mitotic germ cell cycle arrest upon IR

Worms were irradiated with 0 and 60 Gy at the late L4 larval stage as described previously 10. 16 hours post-irradiation, worms were mounted on 3% agar pads and paralyzed with 60 nM NaN_3 for DIC microscopy and the distal region of the germline was scored for number of nuclei in all focal planes within a defined area of 2 μm x 6 μm.

Statistical analysis

Statistical analysis was performed using Excel (Microsoft). Statistical significance was calculated with two-tailed paired Student's t-test. Box plots were generated using BoxPlotR 53. Centre lines show the medians; box limits indicate the 25th and 75th percentiles as determined by R software; whiskers extend 1.5 times the interquartile range from the 25th and 75th percentiles, outliers are represented by dots. The notches are defined as +/-1.58*IQR/sqrt(n) and represent the 95% confidence interval for each median. Non-overlapping notches give roughly 95% confidence that two medians differ.

Supplementary Material

Refer to Web version on PubMed Central for supplementary material.

Acknowledgements

We thank Y. Kohara, M. Marr, the *Caenorhabditis* Genetics Center (funded by the NIH National Center for Research Resources), the Bloomington Stock Center, the Dana-Farber Cancer Institute, Addgene and Geneservice Ltd for antibodies, plasmids, cDNAs, and strains; Agata Lisowski and Ela Stellbrink for technical help. We thank André Franz and Aljona Gutschmidt for critical reading of the manuscript. We thank Kristijan Ramadan and Yossi Shiloh for insightful discussions on the project and exchange of unpublished results. This work was supported by a Wellcome Trust Senior Research award (090944/Z/09/Z) to AG, grants of the German-Israeli Foundation (GIF 1104-68.11/2010), the Deutsche Forschungsgemeinschaft (EXC 229, SFB 829, SFB 670, and KFO 286), the European Research Council (ERC Starting grant 260383), Marie Curie (FP7 ITN CodeAge 316354, aDDRess 316390, MARRIAGE 316964), and the Bundesministerium für Forschung und Bildung (Sybacol FKZ0315893A-B) to B.S., and the Deutsche Forschungsgemeinschaft (EXC 229, HO 2541/8-1, and KFO 286) and the European Research Council (consolidator grant 616499) to T.H. In addition, this work was supported by COST Action (PROTEOSTASIS BM1307), supported by COST (European Cooperation in Science and Technology).

References

1. Hoeijmakers JH. Genome maintenance mechanisms for preventing cancer. Nature. 2001; 411:366–374. DOI: 10.1038/35077232 [PubMed: 11357144]
2. Clejan I, Boerckel J, Ahmed S. Developmental modulation of nonhomologous end joining in Caenorhabditis elegans. Genetics. 2006; 173:1301–1317. DOI: 10.1534/genetics.106.058628 [PubMed: 16702421]
3. Lemmens BB, Tijsterman M. DNA double-strand break repair in Caenorhabditis elegans. Chromosoma. 2011; 120:1–21. DOI: 10.1007/s00412-010-0296-3 [PubMed: 21052706]
4. Bizard AH, Hickson ID. The dissolution of double Holliday junctions. Cold Spring Harb Perspect Biol. 2014; 6:a016477.doi: 10.1101/cshperspect.a016477 [PubMed: 24984776]
5. Matos J, West SC. Holliday junction resolution: regulation in space and time. DNA Repair (Amst). 2014; 19:176–181. DOI: 10.1016/j.dnarep.2014.03.013 [PubMed: 24767945]
6. Schwartz EK, Heyer WD. Processing of joint molecule intermediates by structure-selective endonucleases during homologous recombination in eukaryotes. Chromosoma. 2011; 120:109–127. DOI: 10.1007/s00412-010-0304-7 [PubMed: 21369956]
7. West SC, et al. Resolution of Recombination Intermediates: Mechanisms and Regulation. Cold Spring Harbor symposia on quantitative biology. 2015; doi: 10.1101/sqb.2015.80.027649
8. Bailly AP, et al. The Caenorhabditis elegans homolog of Gen1/Yen1 resolvases links DNA damage signaling to DNA double-strand break repair. PLoS genetics. 2010; 6doi: 10.1371/journal.pgen.1001025
9. Silva N, Adamo A, Santonicola P, Martinez-Perez E, Volpe LA. Pro-crossover factors regulate damage-dependent apoptosis in the Caenorhabditis elegans germ line. Cell Death & Differentiation. 2013; 20:1209–1218. DOI: 10.1038/cdd.2013.68 [PubMed: 23832114]
10. Gartner A, Milstein S, Ahmed S, Hodgkin J, Hengartner MO. A conserved checkpoint pathway mediates DNA damage--induced apoptosis and cell cycle arrest in C. elegans. Molecular cell. 2000; 5:435–443. DOI: 10.1016/s1097-2765(00)80438-4 [PubMed: 10882129]
11. Schumacher B, Hofmann K, Boulton S, Gartner A. The C. elegans homolog of the p53 tumor suppressor is required for DNA damage-induced apoptosis. Current biology : CB. 2001; 11:1722–1727. DOI: 10.1016/S0960-9822(01)00534-6 [PubMed: 11696333]
12. Derry WB, Putzke AP, Rothman JH. Caenorhabditis elegans p53: role in apoptosis, meiosis, and stress resistance. Science. 2001; 294:591–595. DOI: 10.1126/science.1065486 [PubMed: 11557844]
13. Schumacher B, et al. Translational repression of C. elegans p53 by GLD-1 regulates DNA damage-induced apoptosis. Cell. 2005; 120:357–368. DOI: 10.1016/j.cell.2004.12.009 [PubMed: 15707894]
14. Reinke V, et al. A global profile of germline gene expression in C. elegans. Molecular cell. 2000; 6:605–616. DOI: 10.1016/S1097-2765(00)00059-9 [PubMed: 11030340]
15. Vermezovic J, Stergiou L, Hengartner MO, d'Adda di Fagagna F. Differential regulation of DNA damage response activation between somatic and germline cells in Caenorhabditis elegans. Cell death and differentiation. 2012; 19:1847–1855. DOI: 10.1038/cdd.2012.69 [PubMed: 22705849]

16. Johnson ES, Ma PCM, Ota IM, Varshavsky A. A Proteolytic Pathway That Recognizes Ubiquitin as a Degradation Signal. Journal of Biological Chemistry. 1995; 270:17442–17456. DOI: 10.1074/jbc.270.29.17442 [PubMed: 7615550]
17. Koegl M, et al. A novel ubiquitination factor, E4, is involved in multiubiquitin chain assembly. Cell. 1999; 96:635–644. [PubMed: 10089879]
18. Saeki Y, Tayama Y, Toh-e A, Yokosawa H. Definitive evidence for Ufd2-catalyzed elongation of the ubiquitin chain through Lys48 linkage. Biochemical and biophysical research communications. 2004; 320:840–845. DOI: 10.1016/j.bbrc.2004.05.216 [PubMed: 15240124]
19. Hoppe T. Multiubiquitylation by E4 enzymes: 'one size' doesn't fit all. Trends Biochem Sci. 2005; 30:183–187. DOI: 10.1016/j.tibs.2005.02.004 [PubMed: 15817394]
20. Akutsu M, Dikic I, Bremm A. Ubiquitin chain diversity at a glance. Journal of cell science. 2016; 129:875–880. DOI: 10.1242/jcs.183954 [PubMed: 26906419]
21. Kuhlbrodt K, et al. The Machado-Joseph disease deubiquitylase ATX-3 couples longevity and proteostasis. Nat Cell Biol. 2011; 13:273–281. DOI: 10.1038/ncb2200 [PubMed: 21317884]
22. Okumura F, Hatakeyama S, Matsumoto M, Kamura T, Nakayama KI. Functional regulation of FEZ1 by the U-box-type ubiquitin ligase E4B contributes to neuritogenesis. The Journal of biological chemistry. 2004; 279:53533–53543. DOI: 10.1074/jbc.M402916200 [PubMed: 15466860]
23. Hodgkin J, Horvitz HR, Brenner S. Nondisjunction Mutants of the Nematode CAENORHABDITIS ELEGANS. Genetics. 1979; 91:67–94. [PubMed: 17248881]
24. Rape M, et al. Mobilization of processed, membrane-tethered SPT23 transcription factor by CDC48(UFD1/NPL4), a ubiquitin-selective chaperone. Cell. 2001; 107:667–677. [PubMed: 11733065]
25. Richly H, et al. A series of ubiquitin binding factors connects CDC48/p97 to substrate multiubiquitylation and proteasomal targeting. Cell. 2005; 120:73–84. DOI: 10.1016/j.cell.2004.11.013 [PubMed: 15652483]
26. Meerang M, et al. The ubiquitin-selective segregase VCP/p97 orchestrates the response to DNA double-strand breaks. Nat Cell Biol. 2011; 13:1376–1382. DOI: 10.1038/ncb2367 [PubMed: 22020440]
27. Acs K, et al. The AAA-ATPase VCP/p97 promotes 53BP1 recruitment by removing L3MBTL1 from DNA double-strand breaks. Nat Struct Mol Biol. 2011; 18:1345–1350. DOI: 10.1038/nsmb.2188 [PubMed: 22120668]
28. Dantuma NP, Hoppe T. Growing sphere of influence: Cdc48/p97 orchestrates ubiquitin-dependent extraction from chromatin. Trends Cell Biol. 2012; 22:483–491. DOI: 10.1016/j.tcb.2012.06.003 [PubMed: 22818974]
29. Park Y, Yoon SK, Yoon J-BB. TRIP12 functions as an E3 ubiquitin ligase of APP-BP1. Biochemical and biophysical research communications. 2008; 374:294–298. DOI: 10.1016/j.bbrc.2008.07.019 [PubMed: 18627766]
30. Liu G, Rogers J, Murphy CT, Rongo C. EGF signalling activates the ubiquitin proteasome system to modulate C. elegans lifespan. The EMBO journal. 2011; 30:2990–3003. DOI: 10.1038/emboj.2011.195 [PubMed: 21673654]
31. Shaye DD, Greenwald I. OrthoList: a compendium of C. elegans genes with human orthologs. PloS one. 2011; 6doi: 10.1371/journal.pone.0020085
32. Marechal A, Zou L. RPA-coated single-stranded DNA as a platform for post-translational modifications in the DNA damage response. Cell research. 2015; 25:9–23. DOI: 10.1038/cr.2014.147 [PubMed: 25403473]
33. Boulton SJ, et al. BRCA1/BARD1 orthologs required for DNA repair in Caenorhabditis elegans. Curr Biol. 2004; 14:33–39. [PubMed: 14711411]
34. Solinger JA, Kiianitsa K, Heyer WD. Rad54, a Swi2/Snf2-like recombinational repair protein, disassembles Rad51:dsDNA filaments. Mol Cell. 2002; 10:1175–1188. [PubMed: 12453424]
35. Hofmann ER, et al. Caenorhabditis elegans HUS-1 is a DNA damage checkpoint protein required for genome stability and EGL-1-mediated apoptosis. Current biology : CB. 2002; 12:1908–1918. [PubMed: 12445383]

36. Horvitz HR. Genetic control of programmed cell death in the nematode Caenorhabditis elegans. Cancer Res. 1999; 59:1701s–1706s. [PubMed: 10197583]
37. Lee MH, Schedl T. Identification of in vivo mRNA targets of GLD-1, a maxi-KH motif containing protein required for C. elegans germ cell development. Genes & development. 2001; 15:2408–2420. DOI: 10.1101/gad.915901 [PubMed: 11562350]
38. Doh JH, Jung Y, Reinke V, Lee M-HH. C. elegans RNA-binding protein GLD-1 recognizes its multiple targets using sequence, context, and structural information to repress translation. Worm. 2013; 2doi: 10.4161/worm.26548
39. Huang F, Mazin AV. A small molecule inhibitor of human RAD51 potentiates breast cancer cell killing by therapeutic agents in mouse xenografts. PloS one. 2014; 9doi: 10.1371/journal.pone.0100993
40. Park Y, Yoon SK, Yoon J-BB. The HECT domain of TRIP12 ubiquitinates substrates of the ubiquitin fusion degradation pathway. The Journal of biological chemistry. 2009; 284:1540–1549. DOI: 10.1074/jbc.M807554200 [PubMed: 19028681]
41. Gudjonsson T, et al. TRIP12 and UBR5 suppress spreading of chromatin ubiquitylation at damaged chromosomes. Cell. 2012; 150:697–709. DOI: 10.1016/j.cell.2012.06.039 [PubMed: 22884692]
42. Krona C, et al. Screening for gene mutations in a 500 kb neuroblastoma tumor suppressor candidate region in chromosome 1p; mutation and stage-specific expression in UBE4B/UFD2. Oncogene. 2003; 22:2343–2351. DOI: 10.1038/sj.onc.1206324 [PubMed: 12700669]
43. Carén H, Holmstrand A, Sjöberg RMM, Martinsson T. The two human homologues of yeast UFD2 ubiquitination factor, UBE4A and UBE4B, are located in common neuroblastoma deletion regions and are subject to mutations in tumours. European journal of cancer (Oxford, England : 1990). 2006; 42:381–387. DOI: 10.1016/j.ejca.2005.09.030
44. Zage PE, et al. UBE4B levels are correlated with clinical outcomes in neuroblastoma patients and with altered neuroblastoma cell proliferation and sensitivity to epidermal growth factor receptor inhibitors. Cancer. 2013; 119:915–923. DOI: 10.1002/cncr.27785 [PubMed: 22990745]
45. Kloppsteck P, Ewens CA, Forster A, Zhang X, Freemont PS. Regulation of p97 in the ubiquitin-proteasome system by the UBX protein-family. Biochim Biophys Acta. 2012; 1823:125–129. DOI: 10.1016/j.bbamcr.2011.09.006 [PubMed: 21963883]
46. Brenner S. The genetics of Caenorhabditis elegans. Genetics. 1974; 77:71–94. [PubMed: 4366476]
47. Zeiser E, Frøkjær-Jensen C, Jorgensen E, Ahringer J. MosSCI and gateway compatible plasmid toolkit for constitutive and inducible expression of transgenes in the C. elegans germline. PloS one. 2011; 6doi: 10.1371/journal.pone.0020082
48. Praitis V, Casey E, Collar D, Austin J. Creation of low-copy integrated transgenic lines in Caenorhabditis elegans. Genetics. 2001; 157:1217–1226. [PubMed: 11238406]
49. Timmons L, Fire A. Specific interference by ingested dsRNA. Nature. 1998; 395:854.doi: 10.1038/27579 [PubMed: 9804418]
50. Gumienny TL, Lambie E, Hartwieg E, Horvitz HR, Hengartner MO. Genetic control of programmed cell death in the Caenorhabditis elegans hermaphrodite germline. Development (Cambridge, England). 1999; 126:1011–1022.
51. Hengartner MO, Ellis RE, Horvitz HR. Caenorhabditis elegans gene ced-9 protects cells from programmed cell death. Nature. 1992; 356:494–499. DOI: 10.1038/356494a0 [PubMed: 1560823]
52. Hoogewijs D, Houthoofd K, Matthijssens F, Vandesompele J, Vanfleteren JR. Selection and validation of a set of reliable reference genes for quantitative sod gene expression analysis in C. elegans. BMC molecular biology. 2008; 9:9.doi: 10.1186/1471-2199-9-9 [PubMed: 18211699]
53. Spitzer M, Wildenhain J, Rappsilber J, Tyers M. BoxPlotR: a web tool for generation of box plots. Nature methods. 2014; 11:121–122. DOI: 10.1038/nmeth.2811 [PubMed: 24481215]

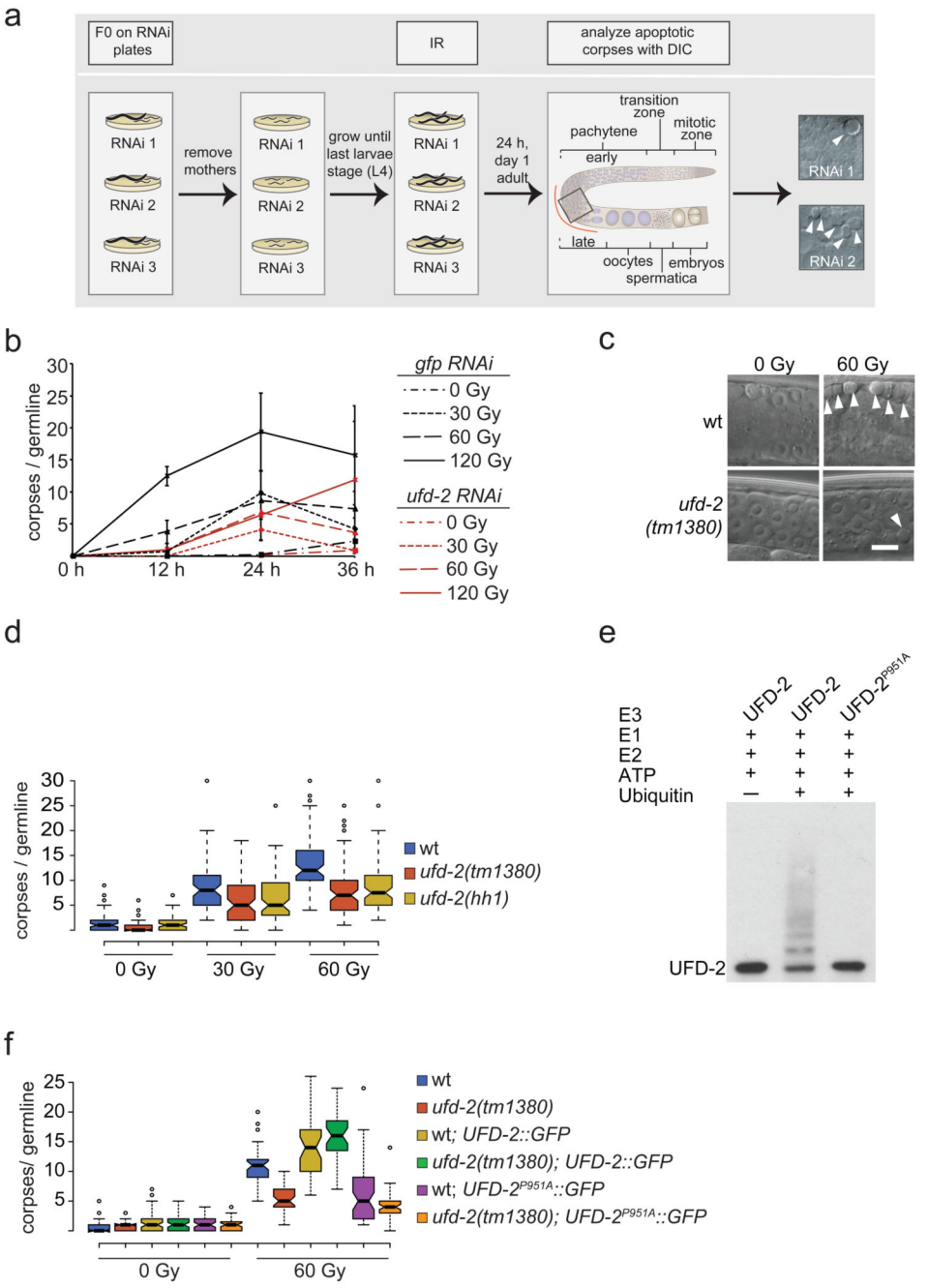

Figure 1.

Ubiquitin ligase activity of UFD-2 is required for apoptosis execution. **(a)** Schematic illustration of RNAi screen for identification of DNA damage-induced apoptosis mediators. After RNAi treatment worms were subjected to IR and scored for apoptotic corpses (indicated by filled arrowheads) 24 hrs later by differential interference contrast (DIC) microscopy. **(b)** Worms treated with indicated RNAi constructs were exposed to IR of increasing dose and scored for apoptotic corpses 24 hrs after treatment. Data represent mean ± s.e.m. of selected data of RNAi screen. **(c)** Representative images of late pachytene cells

Europe PMC Funders Author Manuscripts

Europe PMC Funders Author Manuscripts

of *C. elegans* germline 24 hrs after IR treatment. Filled arrowheads indicate an apoptotic corpse. Scale bar 5 μm. **(d)** Indicated genotypes were scored for DNA damage induced apoptosis 24 hrs after IR. Center lines show the medians; box limits indicate the 25th and 75th percentiles as determined by R software; whiskers extend 1.5 times the interquartile range from the 25th and 75th percentiles, outliers are represented by dots. The notches are defined as +/- 1.58*IQR/sqrt(n) and represent the 95% confidence interval for each median. Non-overlapping notches give roughly 95% confidence that two medians differ. Sample points of 5 independent experiments. **(e)** Auto-ubiquitylation of UFD-2. Ubiquitylation reactions were carried out as indicated using UFD-2 (wild-type) and UFD-2^{P951A} as ubiquitin ligases. Representative immunoblot of 3 independent experiments. **(f)** Indicated genotypes were scored for DNA damage induced apoptosis 24 hrs after IR. Sample points of 3 independent experiments. For *n*-values see Supplementary Table 1.

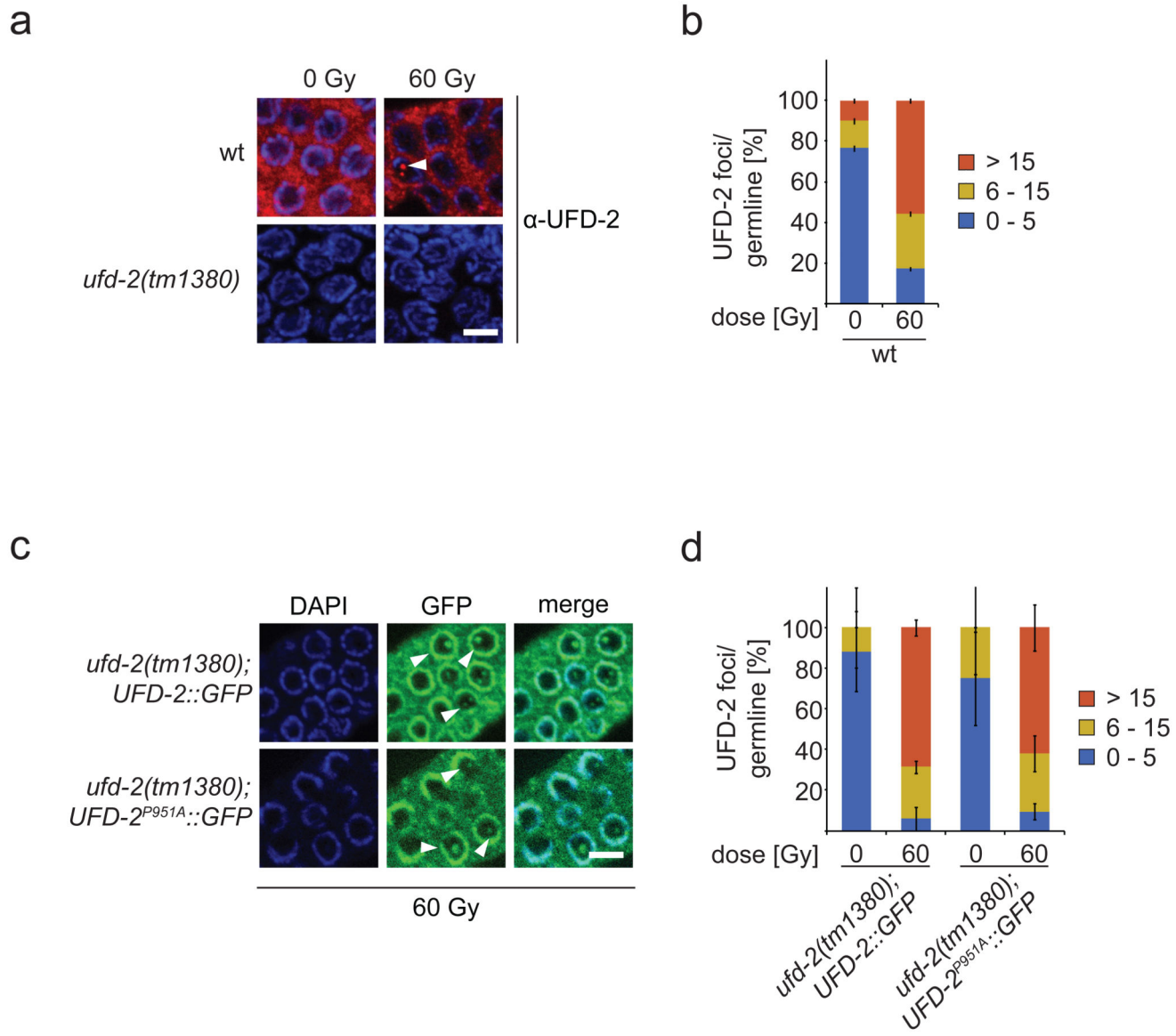

Figure 2.

UFD-2 forms foci late after IR treatment. **(a)** Representative images of worm germlines of indicated genotypes irradiated with 60 Gy IR and stained with α-UFD-2 antibody and DAPI 24 hrs later. Filled arrowhead indicated nucleus with UFD-2 foci. Scale bar, 5 μm and **(b)** corresponding quantification of UFD-2 foci in pachytene region of germlines. Data show means ± s.e.m. of 12 independent experiments. **(c)** Representative images of worm germlines of indicated genotypes irradiated with 60 Gy IR. Germlines were isolated and stained with GFP-booster and DAPI 24 hrs after IR. Filled arrowheads indicate nuclei with UFD-2 foci. Scale bar, 5 μm and **(d)** corresponding quantification of UFD-2 foci in pachytene region of germlines. Data show means ± s.e.m. of 3 independent experiments. For *n*-values see Supplementary Table 1.

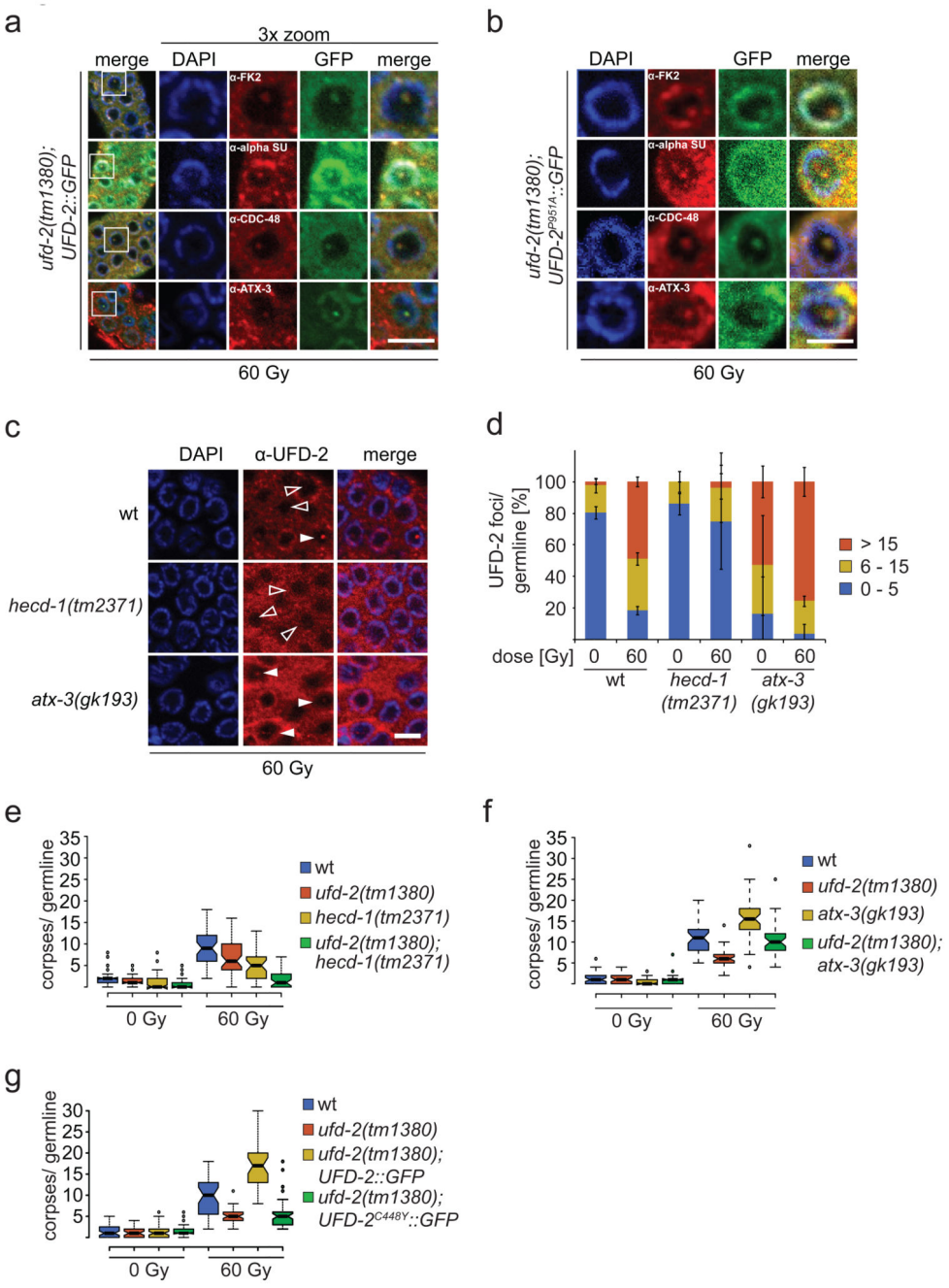

Figure 3.

UPS factors accumulate in UFD-2 hubs and balance apoptotic signalling. Representative images of **(a)** *ufd-2(tm1380); ufd-2::gfp* and **(b)** *ufd-2(tm1380); ufd-2^{P951A}::gfp* immunostained with indicated antibodies. Germlines were isolated 24 hrs after treatment with 60 Gy. DNA stained with DAPI. The boxed area is three times magnified (3x zoom). α-alpha SU, α-Proteasome 20S alpha subunits. Scale bars, 5 μm. Representative images of 3 independent experiments. **(c)** Representative images of worm germlines of indicated genotypes irradiated with 60 Gy IR and stained with α-UFD-2 antibody and DAPI 24 hrs

later. Empty and filled arrowhead indicated nuclei positive or negative for UFD-2 foci, respectively. Scale bar, 5 μm and **(d)** corresponding quantification of UFD-2 foci in pachytene region of germlines. Data show means ± s.e.m. of 3 independent experiments. **(e, f and g)** Indicated genotypes were scored for apoptosis 24 hrs after 60 Gy IR. Sample points of 3 independent experiments. For *n*-values see Supplementary Table 1.

Europe PMC Funders Author Manuscripts

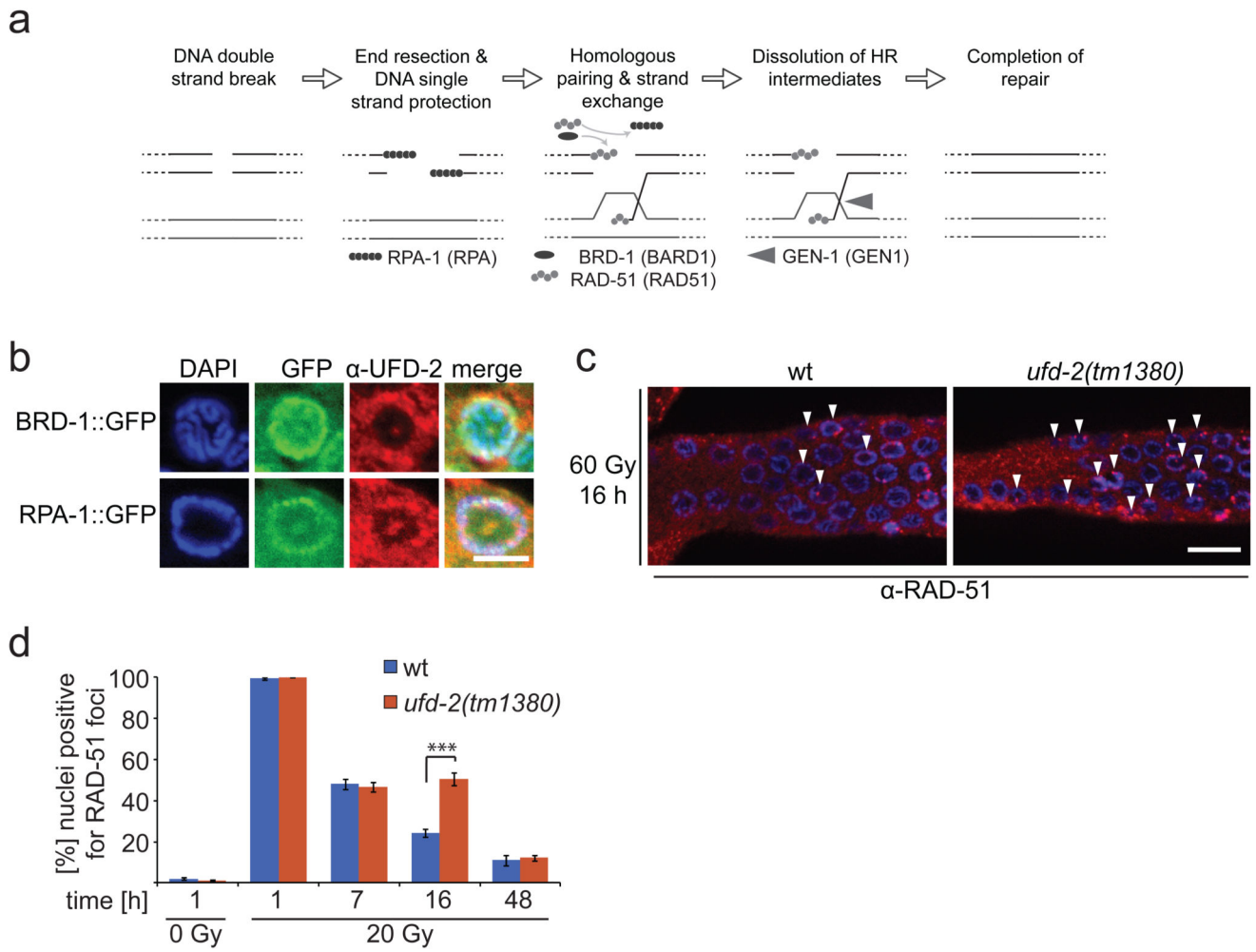

Figure 4.

Loss of *ufd-2* delays DSB repair processing. **(a)** Schematic illustration of DNA DSB repair by HR in *C. elegans*. Upon DSB induction RPA binds resected single stranded DNA, BRD-1 acts together with BRCA-1 at DSB site, RPA is exchanged for RAD-51, which mediates strand invasion, Gen-1 resolves HJ resulting in repaired DSB. Names in brackets indicate human homologues. **(b)** Representative images of *brd-1::gfp* and *rpa-1::gfp* germlines isolated and stained with α-UFD-2 and DAPI 24 hrs after treatment with 60 Gy of IR. Scale bar, 5 μm. Representative images of 3 independent experiments. **(c)** Representative images of germlines isolated from wild-type and *ufd-2(tm1380)* worms 16 hrs after IR treatment with 20 Gy. Germlines were stained with α-RAD-51 and DAPI. Filled arrowheads indicate nuclei positive for RAD-51 staining. Scale bar, 10 μm. **(d)** Quantification of germ cells that were positive for RAD-51 staining. Wild-type and *ufd-2(tm1380)* worms were treated with 0 or 20 Gy of IR and isolated 1, 7, 16, 48 hrs after treatment (7, 16, 48 hrs only for 60 Gy treated worms) and immunostained with α-RAD-51 and DAPI to stain DNA. The last 50 nuclei of pachytene germ cells prior entering diakinesis were evaluated. Data show means ± s.e.m. of 3 independent experiments. The triple asterisk indicates *P* value of ≤ 0.001 in Student's *t*-test. For *n*-values see Supplementary Table 1.

Europe PMC Funders Author Manuscripts

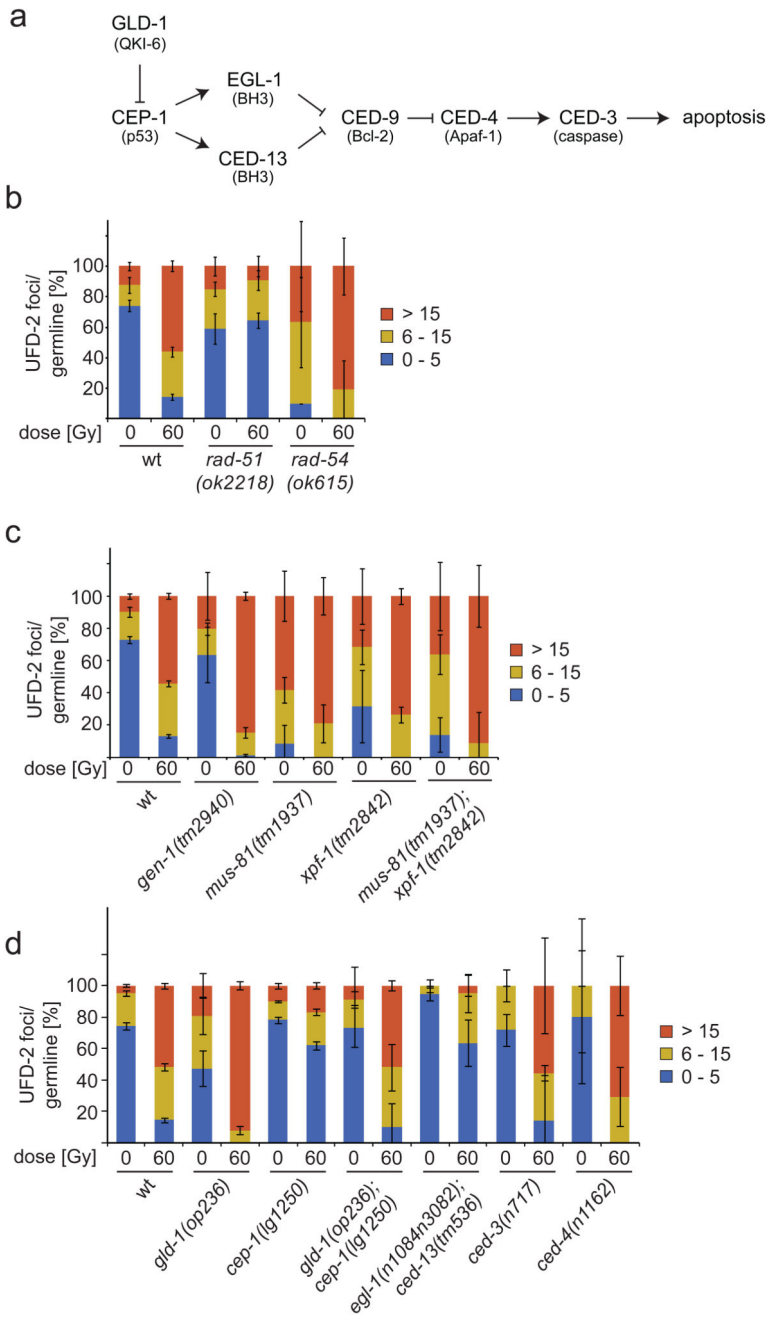

Figure 5.

UFD-2 foci in repair and apoptosis after DNA damage. **(a)** Schematic illustration of apoptosis pathway in *C. elegans*. Names in brackets indicate human homologues. **(b, c and d)** Quantification of UFD-2 foci in pachytene region of germlines of indicated genotypes isolated 24 hrs after irradiation with 60 Gy. Data show means ± s.e.m. of 3 independent experiments. For *n*-values see Supplementary Table 1.

Europe PMC Funders Author Manuscripts

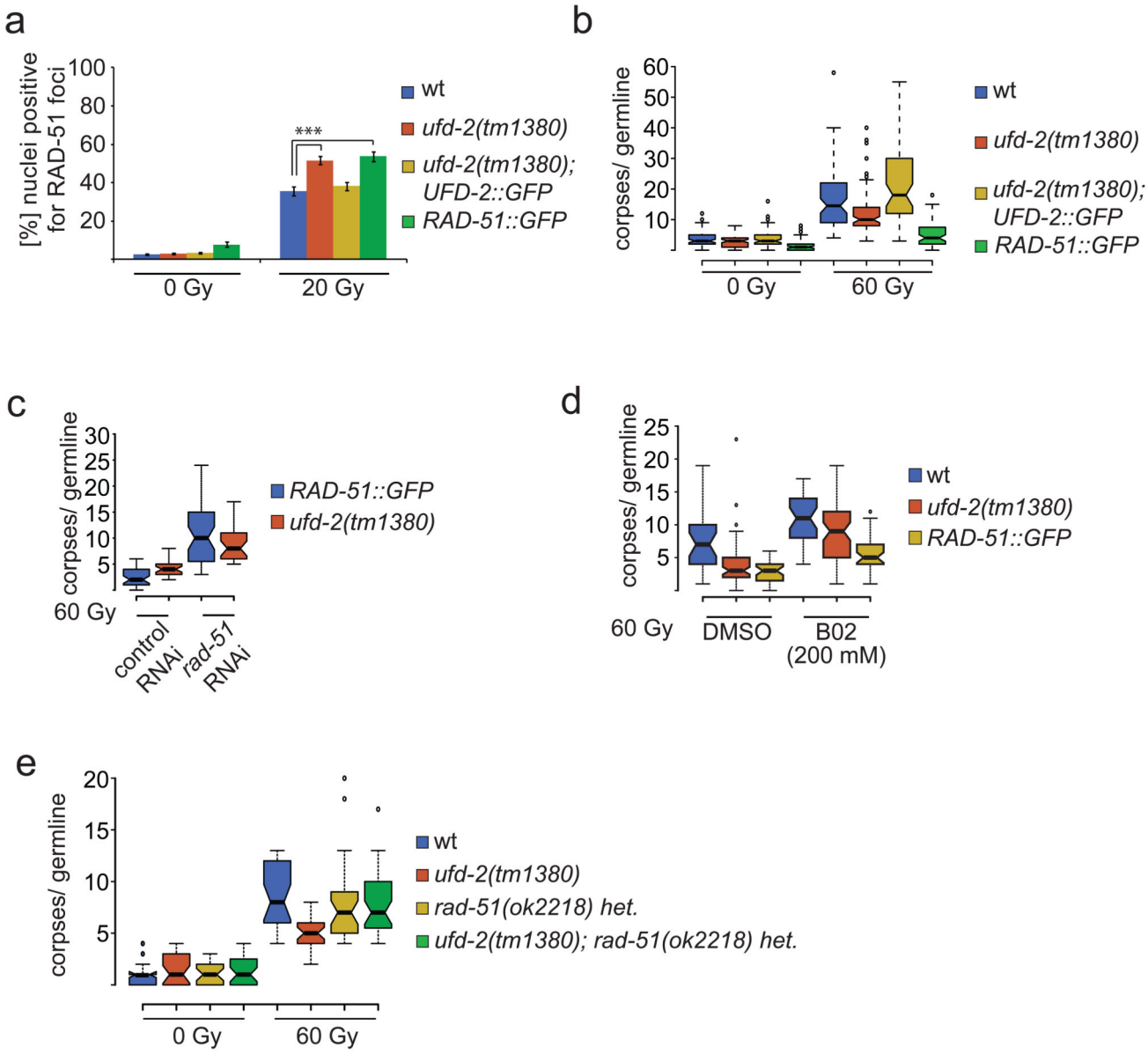

Figure 6.

UFD-2 coordinates communication between repair and apoptosis after DNA damage. **(a)** Quantification of germ cells positive for RAD-51 staining. Worms of indicated genotypes were treated with 0 or 20 Gy of IR. Germlines were isolated 24 hrs after treatment and stained with α-RAD-51 and DAPI. The last 50 nuclei of pachytene germ cells prior entering diakinesis were evaluated. Data show means ± s.e.m. of 3 independent experiments. The triple asterisk indicates *P* value of ≤ 0.001 in Student's *t*-test. **(b)** Indicated genotypes were scored for apoptosis 24 hrs after 60 Gy IR. Sample points of 3 independent experiments. **(c)** *ufd-2* and RAD-51::GFP worms were treated with rad-51 or control RNAi and scored for apoptosis 24 hrs after 60 Gy IR. Sample points of 3 independent experiments. **(d)** wild-type, *ufd-2* and RAD-51::GFP worms were treated with RAD51 inhibitor B02 (200mM) from L1

larvae on and scored for apoptosis 24 hrs after 60 Gy IR. Sample points of 3 independent experiments. **(e)** Indicated genotypes were scored for apoptosis 24 hrs after 60 Gy IR. Sample points of 3 independent experiments. For *n*-values see Supplementary Table 1.

Europe PMC Funders Author Manuscripts

Europe PMC Funders Author Manuscripts

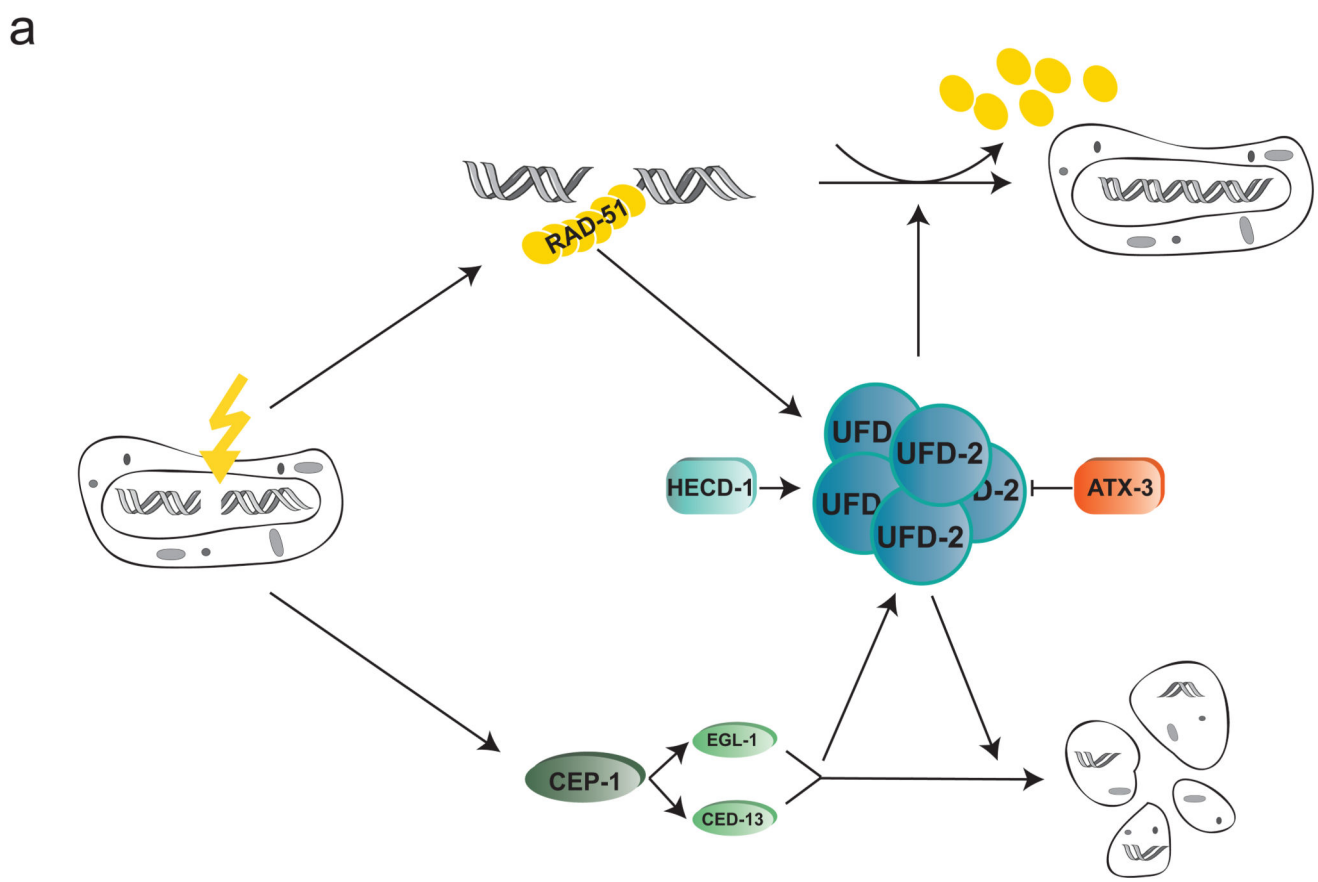

Figure 7.

Model of how UFD-2 integrates HR repair and apoptotic signalling. UFD-2 forms hubs late after IR (additionally containing proteolytic factors as CDC-48 and the proteasome (not shown)) that are dependent on active repair and apoptotic CEP-1 signalling. UFD-2 hub formation is balanced by the E3 ligase HECD-1 and the DUB ATX-3. In accordance with hub formation at later stages after DSB induction, UFD-2 supports RAD-51 dissociation from DSB site at advanced time points and mediates signal to apoptosis pathway.